IEEE Access
Multidisciplinary | Rapid Review | Open Access Journal

SPECIAL SECTION ON DATA-ENABLED INTELLIGENCE FOR DIGITAL HEALTH

Received September 14, 2019, accepted October 7, 2019, date of publication October 11, 2019, date of current version November 15, 2019.

Digital Object Identifier 10.1109/ACCESS.2019.2946932

Localization of Myocardial Infarction With Multi-Lead Bidirectional Gated Recurrent Unit Neural Network

XINGJIN ZHANG[1,2], RUNCHUAN LI[2,3], HONGHUA DAI[2,4], (Member, IEEE), YONGPENG LIU[2], BING ZHOU[2,3], AND ZONGMIN WANG[2,3]

[1]State Key Laboratory of Mathematical Engineering and Advanced Computing, Zhengzhou 450003, China
[2]Cooperative Innovation Center of Internet Healthcare, Zhengzhou University, Zhengzhou 450000, China
[3]Industrial Technology Research Institute, Zhengzhou University, Zhengzhou 450000, China
[4]Institute of Intelligent Systems, Deakin University, Burwood, VIC 3125, Australia

Corresponding author: Zongmin Wang (zmwang@ha.edu.cn)

This work was supported in part by the National Key Research and Development Program of China, under Grant 2017YFB1401200, and in part by the Key Areas Science and Technology Research Program Projects, under Grant 2018AB017.

ABSTRACT Myocardial infarction (MI) is an acute disease. Early detection and early treatment are of great significance for improving the health of people. In order to reduce the misdiagnosis rate of MI diseases, this paper proposes a multi-lead bidirectional gated recurrent unit neural network (ML-BiGRU) learning algorithm based on current research status in the field of intelligent medical diagnosis, combined with the timing and multi-lead correlation characteristics of the electrocardiogram (ECG) signals. At first, the original ECG signal is denoised and preprocessed and then segmented into heartbeats. After that, the heartbeat sequence is sent to the deep neural network training model to learn the classification. Lastly, the Physikalisch-Technische Bundesanstalt (PTB) ECG database is used to verify the multi-lead BiGRU algorithm. The verification results demonstrate that the accuracy of the algorithm for MI localization is 99.84%, which outperform the other algorithms. The experimental results also show that the algorithm is obviously superior to the traditional localization algorithm in improving the localization accuracy, which is of great significance for improving the correct diagnosis rate of MI.

INDEX TERMS Electrocardiogram, myocardial infarction, multi-lead, Bi-GRU.

I. INTRODUCTION

Cardiovascular disease is a serious threat to human health and is gradually becoming a high incidence in China. MI [1] refers to atherosclerotic changes in the coronary arteries of the nutritional myocardium. The cholesterol plaque deposited in the inner wall of the blood vessel detaches and generates thrombus, which blocks a coronary artery so that some of the myocardium does not receive blood supply for a long time. As a result, myocardial ischemia injury and even necrosis occur. MI has very high mortality and disability rate. In the past, the majority of patients with MI were sixty or seventy years old. Nowadays due to the fast pace of life and bad habits, the number of young people suffering from MI is increasing. The best treatment time window for acute MI is 2 hours after onset, commonly known as ''golden 120 minutes'' [2]. If the blocked blood vessels can be opened within 120 minutes and the blood supply to the myocardium is restored, most ischemic myocardium can avoid necrosis.

ECG examination has high accuracy in the diagnosis of MI. It is fast, simple, non-invasive, low in price, and repeatable. ECG is a curve graph of the electric potential change produced by each beat cycle of the heart from the body surface through the electrocardiogram machine. It is a comprehensive manifestation of the heart activity in the body surface, which can reflect the health of the human heart. Some lesions can be reflected by the abnormality of the ECG waveform. Figure 1 is a typical heartbeat waveform of a MI characterized by a significant increase in the ST segment. The ECG signal can be divided into three main parts: the P wave representing the depolarization of the atrial muscle, the QRS complex that occurs during depolarization of the ventricular muscle, and the T wave representing the ventricular repolarization. The U wave not drawn in Figure 1 appears only in certain leads. The

The associate editor coordinating the review of this manuscript and approving it for publication was Linbo Qing.

waveform of the heartbeat will produce different changes for different pathological reasons.

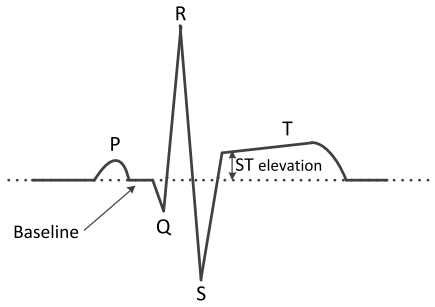

FIGURE 1. A typical waveform of MI heartbeat.

At first, the electrocardiogram can only trace the ECG waveform. The doctor obtains several characteristic values by manual measurement and then judges the disease according to the statistical rules. Later, with the development of computer technology, researchers developed automatic ECG analysis software, which assisted doctors in the time-consuming and repetitive manual recognition process and greatly reduced the doctor's miss-inspection and false detection because of mental fatigue caused by long hours of work. With the aid of automatic analysis software, the doctor analyzes the suspected fragments of the patient's ECG waveform and combines the patient's other physiological examination data to draw the diagnosis conclusion. At present, the electrocardiogram is widely used in clinical practice to assist doctors in identifying and analyzing various heart diseases. A 12-lead ECG is commonly used clinically. It consists of 6 limb leads (I, II, III, aVR, aVL, aVF) and 6 chest leads (V1, V2, V3, V4, V5, V6). The doctor can observe the heart from a different direction and fully understand the electrical activity of the heart. ECG can not only determine the presence or absence of MI but also determine the stage, location, extent, and evolution of the infarction. It can reduce the mortality of patients through timely intervention and treatment. However, this method of analysis is limited by the doctor's clinical experience, so the diagnostic efficiency and accuracy need to be further improved.

ST-segment elevation and series changes of ST-T can be observed in the ECG waveform of MI because the coronary artery is completely blocked by blood clots. However, there is no ST-segment elevation in the ECG waveform of some types of MI because the vessel is not completely blocked. There are only the inverted T wave and the slight ST-segment depression. According to whether the ST-segment is elevated, cardiologists divide MI into ''ST-segment elevation myocardial infarction'' (STEMI) and ''non-ST-segment elevation myocardial infarction'' (NSTEMI). The transmural MI with elevated ST-segment should be sought for urgent percutaneous coronary intervention as quickly as possible. MI with non-ST-segment elevation should be treated with anticoagulant therapy to inhibit platelet activity.

Patients may experience many serious symptoms during MI attacks, such as loss of consciousness, chest pain, and shortness of breath. However, many patients have only mild or no symptoms at all, which is often described as an asymptomatic (also known as silent) heart attack. According to statistics, 22% to 64% of all MIs are silent [3].

The typical characteristics of ECG waveform of MI are: ST segment oblique elevation, T wave towering, ST segment dome-shaped or horizontal elevation, T wave symmetry inversion, symmetry inverted T wave from deep to shallow, T wave returning to normal or no change in the long term, the deeper and wider pathological Q wave. Pathological Q wave or QS wave is caused by necrotic myocardium; an upward elevation of the arch of the ST segment is caused by myocardial damage; inverted T wave is caused by myocardial ischemia.

Based on the hand-crafted features from the ECG signal, researchers at home and abroad have proposed various automatic classification algorithms for MI to assist doctors in making a quick diagnosis. The overall workflow of MI automatic classification includes the following five steps: (1) the ECG signal acquisition; (2) denoising using filtering or wavelet transformation that includes baseline drift, power frequency interference and electromyography (EMG) interference; (3) segmentation into heartbeat; (4) ECG feature extraction and selection; (5) automatic classification and recognition of MI type. The workflow chart is shown in Figure 2.

The traditional method of hand-crafted features uses the QRS complex detection algorithm to locate the R peak first. It then uses a similar method to locate the Q wave start point, the S wave end point, the peak point, the start point and the end point of the P wave and T wave. Finally, it obtains a few amplitude values and interval characteristics. These features are selected according to the doctor's diagnostic rules. This method has a disadvantage. The accuracy of the R-peak detection algorithm is high, but there are still errors. Since other feature values are based on the position extraction of the R wave, these values will produce cumulative errors. Although the detection technology of the QRS complex is relatively mature, it is impossible to effectively detect waveforms such as P wave and T wave. If the corresponding waveform cannot be detected effectively, the patient's condition cannot be accurately diagnosed. At present, the traditional ECG automatic recognition algorithm can only identify several typical MI, and the accuracy rate does not meet the requirements of clinical diagnosis.

Good features can greatly improve the performance of the automatic classification and recognition system of MI. Hand-crafted features rely mainly on the designer's knowledge to manually adjust parameters, and only a small number of parameters are allowed. This is a rather long process and it is difficult to take advantage of big data. The biggest difference between deep learning [4] and traditional recognition methods is that it automatically learns features from big data. It can contain thousands of parameters, quickly learn

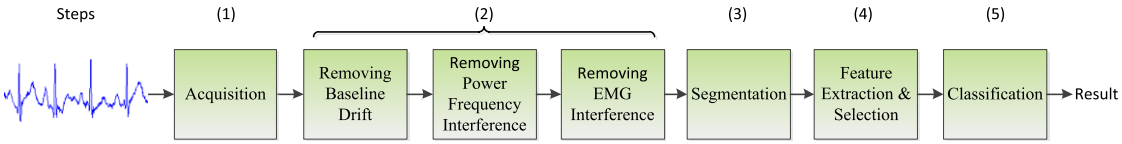

FIGURE 2. MI automatic classification processing procedure based on hand-crafted features.

from training data and mine the hidden useful information from big data. Through multi-layer nonlinear transformation, deep learning automatically learns features from big data, replacing hand-crafted features. The deep learning enables high expressiveness and excellent learning ability and is especially good at extracting complex global features and context information, which is difficult for shallow models. Various implied factors are often associated in a complex, non-linear manner. Deep learning can separate these factors, with different neurons at their highest hidden layers representing different factors, making classification simple. Deep learning has greatly promoted research progress in the fields of image recognition [5], [6], computer vision [7]–[9], speech recognition [10]–[12], etc. It has been applied in the medical field [13]–[16].

At present, most of the methods used in MI detection and localization are the traditional hand-crafted feature extraction methods. With the extensive use of deep learning methods in various fields, more and more researchers use deep learning to extract features automatically to achieve the goal.

In this paper, we proposed a valid and robust method to solve the localization of MI. Classification of MI by automatic feature extraction from 8 leads ECG signal using deep learning framework. The main contributions of this paper are as follows:

1. A neural network deep learning algorithm based on BiGRU and multi-lead ECG signals is proposed for the localization of MI. The temporal relationship between the intra heartbeat and the inter heartbeat is an important evidence in MI localization. The algorithm extracts the effective features hidden in the time sequences from the front and back directions, which improves the accuracy of the localization of MI.

2. Using non-redundant 8-lead ECG signals, each lead is assigned to an independent feature branch, the ML-BiGRU algorithm can learn the different features of different leads. Eight leads constitute an interdependent entity, which aggregates eight feature branches as a whole and uses the full connection layer to predict.

3. A general framework of deep learning is designed, which has a high ability of automatic feature extraction and scalability.

The rest of this paper is organized as follows: Section II describes the work related to the automatic detection and localization of MI; Section III describes the proposed Multi-lead BiGRU algorithm in detail; Section IV describes the experimental process, experimental results, and analysis; the conclusions are given in Section V.

II. RELATED WORK

Due to the significance of early detection diagnosis, the various classification methods have been proposed for automatic analysis and diagnosis of MI. Most methods extract some hand-designed eigenvalues from the morphology and statistics fields after preprocessing the ECG signal, such as P wave amplitude, Q wave amplitude, R wave amplitude, T wave Amplitude, PR interval, QT interval, ST interval, ST amplitude, ST-segment elevation or depression, and RR interval, etc. A classification model is established and the automatic classification of MI diseases is implemented based on these eigenvalues. In order to speed the process, some methods only use single-lead data, which will decrease accuracy. Some methods can only detect the presence or absence of MI, can not achieve more accurate localization. From single-lead to multi-lead, from detection to localization, from hand-crafted to automatic extraction of features, researchers continuously improve the accuracy of MI localization.

Sopic *et al.* [17] use random forest hierarchical classification to achieve detection of MI. Researchers increase the number of features layer by layer to reduce the time required for classification. It is fast and suitable for the real-time analysis system. Sharma *et al.* [18] design a dual-band optimal bi-orthogonal wavelet filter to preprocess the ECG signal, and then use the k-nearest neighbor (KNN) method to implement classification of MI only using single lead. Diker *et al.* [19] use recursive feature elimination (RFE) to select eleven features from morphological and statistical domains and use KNN and artificial neural network (ANN) methods to detect MI. Lui and Chow [20] use the data of the standard I lead on the PTB database to detect the MI using a convolutional recurrent neural network. This MI classifier is used for portable ECG devices. In order to reduce the computational complexity, only single-lead data is used. Acharya *et al.* [21] use the standard II lead ECG data to achieve the detection of MI using the CNN method. To improve the classification speed and reduce the complexity of the algorithm, these MI detection methods only use single-lead ECG signals. However, due to the lack of useful information from other leads, the accuracy of classification is affected.

To improve the MI detection accuracy, effective features are extracted from multi-lead ECG information. Banerjee and Mitral [22] extract QRS_vector from the chest leads V1-V4 and use a simple classification rule method to detect anteroseptal MI in the PTB database. Dohare *et al.* [23] use the principal component analysis (PCA) method to reduce the dimension of the extracted multidimensional features, and

then implement the detection of MI with the SVM method based on radial basis function (RBF). Chang *et al.* [24] use the hidden Markov model (HMM) method to extract the features of V1-V4 chest leads, use SVM and Gaussian mixture model (GMM) to achieve the detection of MI. Bhaskar [25] uses the classical Pan-Tompkins method to identify the R wave and uses the wavelet transform method to extract features. Then the PCA method is used to reduce the dimension. Finally, the ANN and SVM methods are used to complete the detection of MI. Reasat and Shahnaz [26] use the three-lead ECG data to detect the MI using the CNN method. Although these methods improve the accuracy of MI detection, there is still a lack of further MI localization for the needs of clinicians.

Khatun and Morshed [27] use the single lead (V4) of the PTB database to implement the detection and localization of a total of eleven diseases including arrhythmia and MI using the bagging decision tree method. They extract 33 hand-crafted features: 15 interval type and 18 amplitude type. Based on the MI detection, this method adds the MI localization. However, due to the use of only single lead ECG information, there is room for further improvement in the accuracy of MI localization.

The following methods use multi-lead ECG signals, not only to detect whether there is an MI but also to determine the location of MI. Yang *et al.* [28] extract hand-crafted features from the ECG signal. They use the classification and regression tree (CART) method to achieve detection and localization of ECG records of 368 patients with MI and 80 healthy controls. Acharya *et al.* [29] extract 12 nonlinear features. Then they use the KNN method to achieve the detection and localization of MI. Padhy and Dandapat [30] use the SVM method to achieve detection and localization of five types of MI and healthy controls. Sharma *et al.* [31] use SVM and KNN based on RBF kernel to achieve the detection and localization of MI. Strodthoff and Strodthoff [32] use the convolutional neural network (CNN) method to detect and locate the MI on the 8-lead ECG signals of the PTB dataset. Liu *et al.* [33] use the 12-lead ECG data to achieve the detection and localization of MI using CNN method. Wu *et al.* [34] employ the sparse auto-encoder (SAE) to learn deep features from the multi-scale ECG signal. Then the softmax regression is employed to build a multi-class classifier based on the optimal representation. Sun *et al.* [35] extract 72 polynomial coefficients for each heartbeat. They use KNN and support vector machine (SVM) methods to achieve the localization of five types of MI. Arif *et al.* [36] use discrete wavelet transform to detect QRS complexes, extract several time-domain features from the 12-lead ECG signals, and classify them by KNN method to achieve the localization of MI. These methods can improve the accuracy of MI localization by taking into account the multi-lead ECG information. But it takes more time because of increased complexity of the algorithm.

Machine learning methods based on various hand-crafted features are used to detect and locate MI in much literature. The hidden features behind the data are difficult to extract.

TABLE 1. Summary of related work on using ECG signal in detection or localization of MI.

Literatures	leads	Methods	Detection/ Localization
[17]	Single-lead	Random Forest	Detection
[18]		KNN	
[19]		KNN&ANN	
[20][21]		CNN	
[22]	Multi-lead	Rule Tree	Detection
[23]		SVM	
[24]		SVM&GMM	
[25]		ANN&SVM	
[26]		CNN	
[27]	Single-lead	Decision Tree	Detection& Localization
[28]	Multi-lead	CART	Detection& Localization
[29]		KNN	
[30]		SVM	
[31]		SVM&KNN	
[32][33]		CNN	
[34]		SAE	
[35]	Multi-lead	KNN&SVM	Localization
[36]		KNN	

In recent years, with the extensive application of deep learning, it is possible to extract features automatically by machine learning. These [20], [21], [26], [32], [33], [34] methods based on deep learning are applied to the detection and localization of MI by automatically extracting more effective features than those of hand-crafted, but the accuracy still needs to be further improved. Related works are summarized in Table 1.

III. MULTI-LEAD BIDIRECTIONAL GATED RECURRENT UNIT NEURAL NETWORK

The ECG signal is an important basis for the diagnosis of cardiovascular disease. It is an unstable, non-linear and weak electrical signal. Its amplitude is about a few millivolts and its frequency range is between 0.05Hz and 100Hz. So it can be easily interfered by various factors such as human activities and instruments during the process of the signal acquisition, which is not conducive to the feature extraction of the ECG signal. Therefore, it is necessary to filter out various noises of the collected ECG signal. The main noises are sinusoidal baseline drift with frequencies less than 5 Hz due to human breathing, motion, etc., 50 Hz or 60 Hz power frequency interference generated by power transmission, and irregular electromyography due to human muscle contraction interference. Table 2 shows the symbols used in the paper.

A. BASELINE DRIFT

During the ECG signal acquisition process, the baseline drift of the ECG signal may occur due to changes in electrode

TABLE 2. Summary of symbols.

Symbol	Description
X	Sequence of ECG signal
x_t	Input of the current neuron
h_{t-1}	Output of the previous neuron
W_z	Weight of the update gate
σ	Sigmoid function
z_t	Value of the update gate
r_t	Value of reset gate
W_r	Weight of the reset gate
h_t	Output of the current neuron
$\tilde{h}_t$	Candidate output value of the current neuron
W	Weight of the output state

resistance, polarization potential changes of the electrodes, direct current (DC) offset drift of the ECG amplifier, human breathing or muscle slow moving. When the baseline drift is severe, the doctor cannot perform waveform recognition and parameter measurement, which directly affects the accuracy of the clinical diagnosis. The baseline drift is similar to a slowly changing sinusoid with a frequency between 0.05 Hz and 2 Hz, partially overlapping the frequency of the ST segment in the ECG signal, and the ST segment is an important basis for judging MI and myocardial ischemia. Common methods for removing baseline drift are median filtering, high-pass filtering, integer coefficient filtering, curve fitting, morphological processing, wavelet transform, and adaptive filters. Some of these methods will cause large deformation of the ST segment, and some require a long processing time due to high algorithm complexity, and some processing results will have a certain offset. To balance the advantages and disadvantages of various algorithms, this paper chooses a polynomial curve fitting method, which can quickly and better remove the baseline drift.

First, fit the baseline of the drift from the original ECG signal, select the sixth polynomial fit, and fit the data to

$$v_i = c_0 + c_1 z_i + c_2 z_i^2 + \cdots + c_6 z_i^6, \quad i = 1, 2, \cdots, n \tag{1}$$

$\vec{c} = [c_0, c_1, \cdots c_6]^T$ is the parameters to be determined. z_i and v_i are the coordinate value of the data point. The number of data points is n, represent formula (1) as a matrix multiplication form in (2):

$$\begin{bmatrix} 1 & z_1 & \cdots & z_1^6 \\ 1 & z_2 & \cdots & z_2^6 \\ \vdots & \vdots & \ddots & \vdots \\ 1 & z_n & \cdots & z_n^6 \end{bmatrix} \cdot \begin{bmatrix} c_0 \\ c_1 \\ \vdots \\ c_6 \end{bmatrix} = \begin{bmatrix} v_1 \\ v_2 \\ \vdots \\ v_n \end{bmatrix} \tag{2}$$

A brief note is:

$$Z\vec{c} = \vec{v} \tag{3}$$

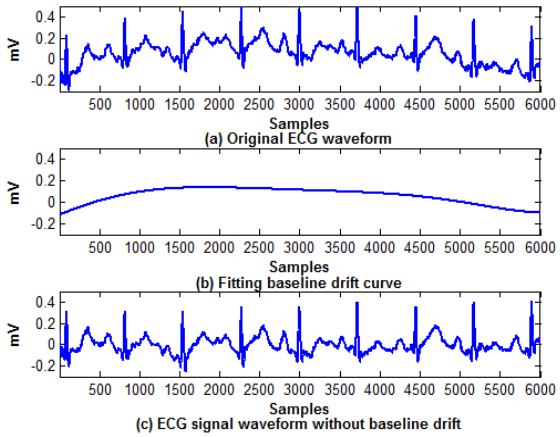

FIGURE 3. Comparison chart before and after baseline drift removal.

Transform the formula (3) for the sake of getting $\vec{c}$.

$$Z^T Z\vec{c} = Z^T\vec{v} \rightarrow \vec{c} = (Z^T Z)^{-1} Z^T\vec{v} \tag{4}$$

The coefficient matrix $\vec{c}$ is obtained, and the fitted baseline drift curve is obtained simultaneously. Then, the fitted curve is subtracted from the original ECG signal, and the ECG signal without baseline drift is extracted. In the following, the ECG signal with baseline drift is displayed. Comparison chart before and after baseline drift removal is shown in Figure 3. (a) represents the original ECG waveform before the baseline drift is removed; (b) represents the baseline drift waveform fitted from the original ECG signal; (c) represents the ECG waveform after the baseline drift is removed. It is apparent from the figure that the drifting signal is pulled back to the same horizontal line.

B. POWER FREQUENCY INTERFERENCE

Power supply networks are ubiquitous. Power frequency interference is the most common and the main source of interference for the ECG signal. It is mainly introduced in the form of displacement current through the capacitive coupling of the input wires of the human body and the measuring system. Its intensity is sufficient to flood the unused ECG signal. The power frequency will fluctuate due to the instability of the power system, and the range of fluctuation is about $\pm 3\%$ of the power frequency. The presence of power frequency noise will greatly reduce the signal-to-noise ratio of the ECG signal. The main methods for removing power frequency interference are smoothing filter, notch filter, wavelet transform method, band-stop filter, and adaptive filter. In this paper, the Infinite Impulse Response (IIR) digital band-stop filter is adopted. The method is simple in principle, good in effect and fast in processing speed. The PTB ECG data was taken from a medical university in Germany with a power frequency interference of 50 Hz. The phase/amplitude-frequency characteristics of the band-stop filter are shown in Figure 4. (a) shows the phase-frequency characteristic of the band-stop filter, with a significant change around 50Hz;

(b) shows the amplitude-frequency characteristic of the band-stop filter. The amplitude around 50 Hz is close to zero. The spectrum of the ECG signal before and after the band-stop filter is shown in Figure 5. (a) shows the spectrum of the original ECG signal, with a significant amplitude around 50 Hz; (b) shows the ECG spectrum of the band-stop filter. The amplitude is close to zero near 50 Hz. The comparison of the ECG signal before and after the removal of power frequency interference is shown in Figure 6. (a) shows the waveform of the original ECG signal, and obvious irregular fluctuations can be seen; (b) shows the ECG waveform after removing the power frequency interference, which is regular. The fluctuations have disappeared.

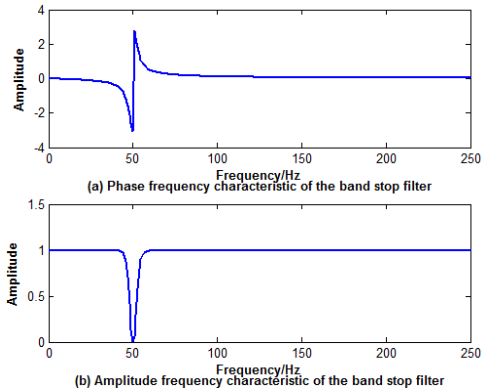

FIGURE 4. Band-stop filter phase/amplitude-frequency characteristic diagram.

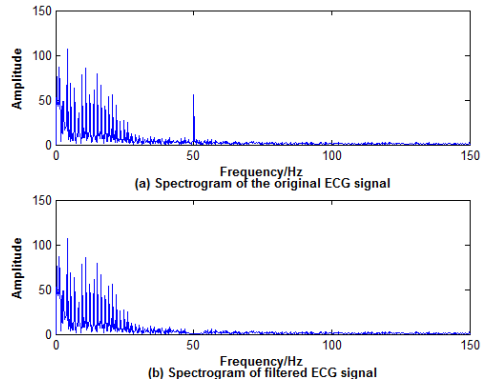

FIGURE 5. Spectrogram of the ECG signal before and after band-stop filtering.

C. EMG INTERFERENCE

The frequency range of EMG interference is very wide, similar to white noise, and it is between 5 Hz and 2000 Hz. To remove irregular EMG interference, the band-stop filtering method is usually adopted. The principle is to set the upper and lower limits of the frequency. The frequency of the input signal is between the upper and lower limits to pass the filter. Signals that exceed or fall below the set threshold will be filtered out. The band-pass filter allows the

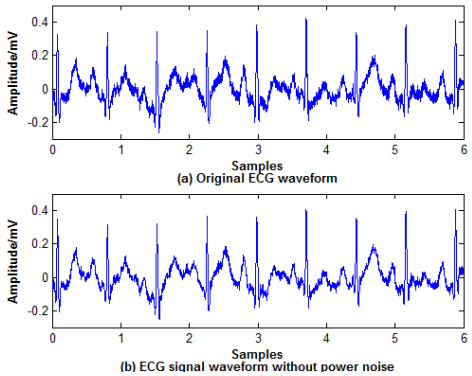

FIGURE 6. Before and after the removal of power frequency interference comparison chart.

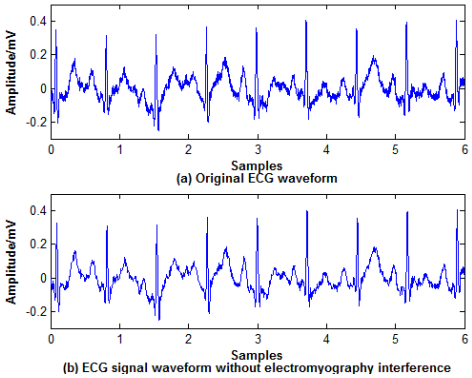

FIGURE 7. Comparison before and after removal of myoelectric interference.

signal to pass through the entire frequency band-pass, and its band-stop attenuates and suppresses the signal. In this paper, a Butterworth digital band-pass filter is used to remove signal components with frequencies below 0.05 Hz or above 100 Hz from the original ECG signal. The squared function of the amplitude of the Butterworth filter is:

$$A^2(\Omega) = |H(j\Omega)|^2 = \frac{1}{1 + (\Omega/\Omega_c)^{2N}} \tag{5}$$

N is an integer, called the order of the filter. Ω is the angular frequency, and Ω_c is the 3dB cutoff frequency of the filter. The larger N is, the steeper the transition zone is, and the better the pass-band and stop-band approximation are. The Butterworth filter is characterized by a maximum flat frequency response curve in the pass-band, no ups and downs, and a gradual drop to zero in the blocking band. The comparison of the ECG signal before and after removal of EMG interference is shown in Figure 7. (a) indicates the waveform of the original ECG signal, and obvious glitch can be seen; (b) indicates the ECG waveform after the band rejection filter, and the glitch disappears.

D. HEARTBEAT SEGMENTATION

The QRS complex of ECG waveform represents the potential changes of the two ventricular excitatory processes. The

excitability generated by the sinus node first reaches the left side of the interventricular septum and then propagates from the inside to the outside according to a certain route and direction. As the various parts of the ventricle are depolarized successively to form multiple instantaneous integrated ECG vectors, the projection on the lead axis of the frontal plane is generated. A typical QRS complex consists of three connected waves. The first downward wave is a Q wave. After the Q wave, a narrow upward wave is an R wave. The R wave is connected to a downward wave. It is an S wave. Since these three waves are closely connected and the total time does not exceed 0.1 seconds, they are collectively called QRS complex. The time taken by the QRS complex represents the time required for ventricular muscle excitation, and the normal person's QRS complex time is between 0.06 and 0.1 seconds. R wave has higher amplitude and larger slope compared with other waveforms in ECG. The center band of QRS complex is about 17Hz and the bandwidth is about 10Hz according to spectrum analysis. These two are distinguishing characteristics of the QRS complex. The QRS complex is usually detected by position, width, amplitude, and frequency. Several representative detection algorithms are listed as follows: detection algorithms based on filtering and threshold, detection algorithms based on a mathematical model, detection algorithms based on wavelet transform and detection algorithms based on neural network. Each algorithm has its own advantages and disadvantages in accuracy and complexity. After compromise, this paper uses the classic Pan-Tompkins [37], [38] algorithm. On the basis of QRS complex detection, heartbeat segmentation can be achieved, so the accuracy of QRS complex detection is directly related to the accuracy of heartbeat segmentation, and ultimately affects the accuracy of MI localization. The accuracy rate of this algorithm is 99.325%. This provides a guarantee for the correctness of heartbeat segmentation and MI localization.

The Pan-Tompkins algorithm is a real-time algorithm based on the differential method and the double threshold method for detection of the QRS complex. To ensure the accuracy of the QRS complex, firstly, the ECG signal passes through a band-pass filter in order to remove various noises. The output data is then differentiated to increase the QRS complex's slope information. After that it passes through squaring to make all the data positive value and further increase the difference between QRS complex peak and other peak. Next, the data is smoothened by using moving window integration. Finally, the decision algorithm is used to judge the threshold of the differential signal and the integrated signal and the QRS complex are detected. The Pan-Tompkins algorithm can automatically update the threshold according to the QRS complex that has been detected before. At the same time, the algorithm also adopts the refractory period technology for the first time to reduce the false detection rate caused by high T waves and also uses the backtracking technique to reduce the missing detection rate caused by the low amplitude QRS complex. The algorithm is simple in principle, fast in processing, and easy to implement in engineering applications.

According to statistics, adults have a heartbeat of about 60 to 100 beats per minute. Considering the elderly and children, if you extract a number of sampling points forward and backward based on the peak point of R, you can basically cover the main features of a heartbeat waveform. In this paper, the R wave peak point is first located, and then the original sample data of 250ms and 400ms are selected forward and backward respectively, and these values are combined into a feature vector of a single heartbeat.

This paper preprocesses the PTB database and extracts 59,451 heartbeats. These heartbeats belong to 11 categories. To remove the type with too few samples, the final experiment used six types of heartbeat data: anterior MI (AMI), anterolateral MI (ALMI), anterior-septal MI (ASMI), inferior MI (IMI), infero-lateral MI (ILMI) and healthy control (HC). Figure 8 shows examples of the AMI, ALMI, ASMI, IMI, ILMI and the HC heartbeat (for the pathological changes are visually apparent in lead V5). A total of 54,753 heartbeats, the number of samples of various types of heartbeats is shown in Table 3. In theory, the learning information will be more comprehensive and overall better results will be obtained if all 15 leads data are used, but this is not in line with clinical practice. Clinically only 12 leads are available. In addition, since the data of the six limb leads is a linear combination of two measured voltages (e.g. I and III), only two limb leads are used. The data from other limb leads are discarded to remove the data correlation [39]. The final experiment in this paper only considers the 8-lead ECG data that is commonly used and not redundant in clinical applications.

To achieve better accuracy in the detection and localization of MI, we introduced a new approach. With the rapid development of sensor, storage, computer, and network technology, the trend of data expansion is ongoing. How to use artificial intelligence technology to acquire implied and hidden information from big data effectively is the most interesting topic in big data analysis. Deep learning changed the traditional machine learning method. With the successful application of deep learning in the digital recognition of MNIST datasets, more and more researchers are beginning to notice and try to apply this new method. At the same time, the development of deep learning technology is changing each day, and the industries involved are also becoming wider and wider. So far, deep learning has shown great advantages in applications such as speech recognition, image understanding, natural language processing, and video recommendation, and has triggered a breakthrough change.

E. MULTI-LEAD BIDIRECTIONAL GATED RECURRENT UNIT

In this paper, a new automatic classification algorithm for MI based on BiGRU and multi-lead ECG signals is proposed. The acquired ECG signal from multi-lead is preprocessed, segmented into heartbeat sequences respectively and then sent to BiGRU network for learning. Softmax layer gets the classification results. According to einthoven's law, if the data

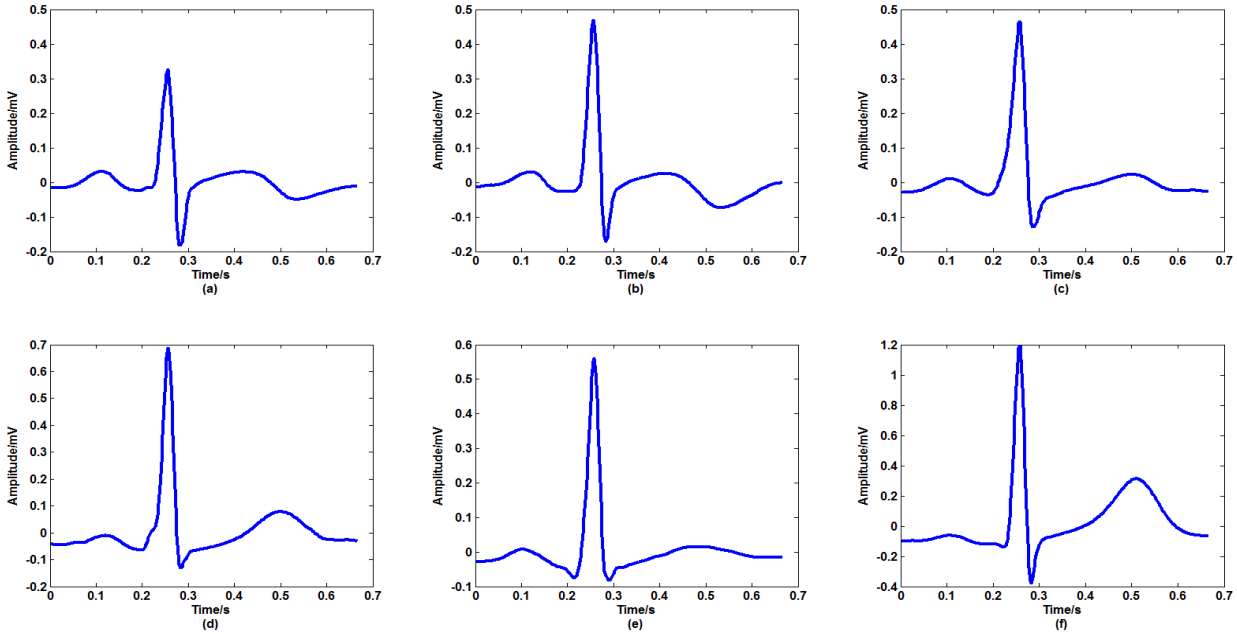

FIGURE 8. Examples of (a) anterior MI, (b) antero-lateral MI, (c) anterior-septal MI, (d) inferior MI, (e) infero-lateral MI and (f) the healthy heartbeat.

TABLE 3. The number of heartbeats in each classification.

classification name	The number of heartbeats
anterior (AMI)	6338
antero-lateral (ALMI)	6554
anterior-septal (ASMI)	11233
inferior (IMI)	12323
infero-lateral (ILMI)	7733
healthy control (HC)	10572
total	**54753**

of limb lead I and III are collected, the remaining four limb leads can be derived from limb lead I and III by the following four formulas [40], [41]:

$$II = I + III \tag{6}$$

$$aVR = -0.5 * (I + II) \tag{7}$$

$$aVL = I - 0.5 * II \tag{8}$$

$$aVF = II - 0.5 * I \tag{9}$$

The data of 6 chest leads are collected directly. It is precise because there are linear correlations among the six limb leads, so we use non-redundant 8 leads (2 limb leads and 6 chest leads) data for deep learning, automatic feature extraction, and finally classification, that is, myocardial infarction location. The classification model architecture diagram is shown in Figure 9.

ECG data is a kind of time series data reflecting human heart health. A series of potential values were obtained by the electrode patches attached to the body at a certain sampling frequency. Similar time sequence application includes speech recognition, stock trading, sensor network monitoring, moving object tracking and so on. In order to meet this demand, the Recurrent Neural Network (RNN) was proposed. A timing structure is added in the RNN, and the output of the neuron can be directly applied to itself at the next timestamp. RNN can be thought of as a neural network that passes over time. Its depth is the length of time. Unfortunately, vanishing gradient problem occur on the timeline. To solve this problem, the long short-term memory (LSTM) [42] is proposed by Hochreiter and Schmidhuber (1997). It includes input, output and forget gate, ranging from 0 to 1, which is equivalent to weighted learning of input and output, and automatic learning of weighted parameters using a large amount of data. The gate is switched to realize the temporal memory function. The gate can selectively pass information and prevent the gradient from disappearing.

LSTM is proposed in order to overcome the difficulty that RNN can't handle long-distance dependence well. However, the form of the LSTM neural network model is more complicated, and there are also problems like long training and prediction time. The GRU proposed by Chung *et al.* [43] maintains the effect of LSTM while making the structure simpler, so it is very popular. Figure 10 shows GRU neuron structure, which is a variant of the LSTM, It merges the input gate and forget gate in LSTM into an updated gate, and replaces it with a reset gate. The update gate is used to control the degree to which the status information of the previous moment is brought into the current state. The larger the value of the update gate, the more the status information of the previous moment is brought in. The reset gate is used to control the degree of ignoring the status information of the previous moment. The smaller the value of the reset gate, the more neglected. What is special about these two gating mechanisms is that they are capable of storing information in long-term sequences that are not cleared over time and

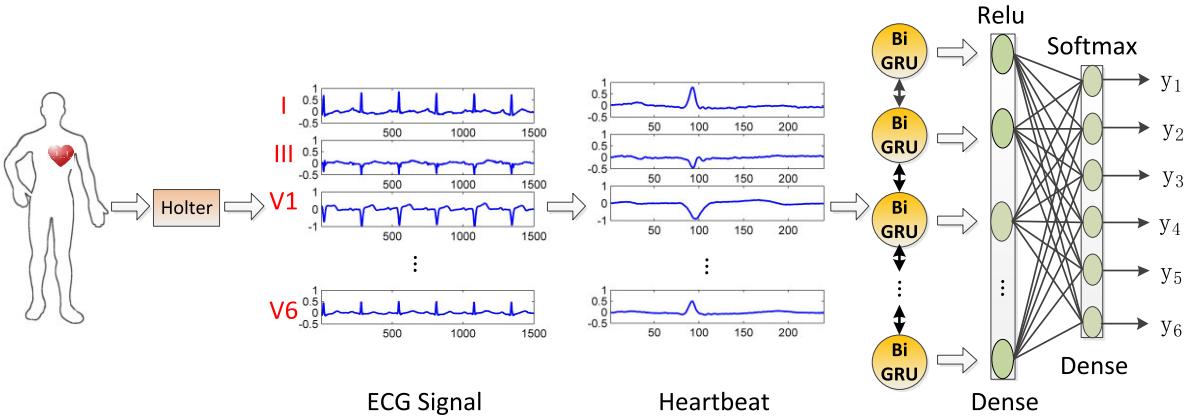

FIGURE 9. Automatic MI classification model architecture.

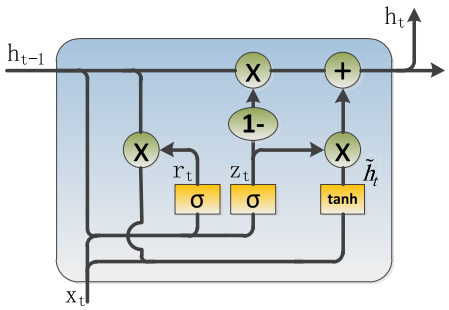

FIGURE 10. GRU neuron structure.

are not removed because they are not relevant to prediction. If the reset gate is set to 1 and the update gate is set to 0, it degenerates into a standard RNN model.

$$z_t = \sigma\left(W_z \cdot [h_{t-1}, x_t]\right) \tag{10}$$

$$r_t = \sigma\left(W_r \cdot [h_{t-1}, x_t]\right) \tag{11}$$

$$\tilde{h}_t = \tanh\left(W \cdot [r_t * h_{t-1}, x_t]\right) \tag{12}$$

$$h_t = (1 - z_t) * h_{t-1} + z_t * \tilde{h}_t \tag{13}$$

h_{t-1} represents the output of the previous neuron. x_t represents the input of the current neuron. W_z represents the weight of the update gate. σ represents the sigmoid function. By adding the output of the previous neuron and the input of the current neuron, then multiplying by the weight of the update gate the value of the update gate z_t is obtained by using the sigmoid function. The update gate controls the information at the time before the update gate is brought to the current hidden state. The larger the value of update gate is, the more information is provided by the hidden node at the previous time. r_t represents the reset gate. W_r represents the weight of the reset gate. By adding the output of the previous neuron and the input of the current neuron, then multiplying by the weight of the reset gate, the value of the reset gate r_t is obtained by using the sigmoid function. When the value of the reset gate is close to 0, it means to ignore the information of the hidden node before, and only input the current information as input. This mechanism can make the model discard some useless information about the previous neuron. $\tilde{h}_t$ represents the candidate output value of the current neuron. W represents the weight of the output state. tanh represents the hyperbolic tangent function. By multiplying the output of the previous neuron and the value of the reset gate, adding by the input of the current neuron, and then multiplying the weight of output state. The value of the $\tilde{h}_t$ is obtained by using the hyperbolic tangent function. By subtracting the value of the reset gate from 1, multiplying by the output of the previous neuron, and then adding the product of the value of update gate and the candidate output value of the current neuron, the value of h_t is obtained. Each hidden unit has an independent reset gate and update gate, and can automatically learn the dependencies of different time ranges. In general, the reset gate that learns the short-distance dependency hidden node will be active, and the update gate that learns the long-distance dependency hidden node will be more active.

The state of the transmission is one-way from front to back in RNN. However, in some cases, the output of the current moment is not only related to the past state but also related to the future state. In order to determine the category of current heartbeat, it is necessary to refer to the two or three waveforms both after and before the current heartbeat, according to the experience of clinicians. A bidirectional RNN (BiRNN) is needed to solve such problems. In order to use the past and future information from the current time, BiRNN will supply two RNNs in opposite directions at the same time, while the output is determined by the two one-way RNNs. The replacement of the RNN in the bidirectional RNN with the LSTM or GRU structure constitutes BiLSTM and BiGRU.

The BiGRU structural model is shown in Figure 11. A circle is used to represent a GRU unit. A basic unit of BiGRU consists of a pair of forward-propagating GRU units and a backward-propagating GRU unit, and several BiGRU basic units are stacked to form a BiGRU deep learning network. At any time, the input of the current hidden layer GRU unit has two sources, one is the information $\vec{h}_{t-1}^{(i)}$ transmitted from the hidden layer at the previous moment. The other is the

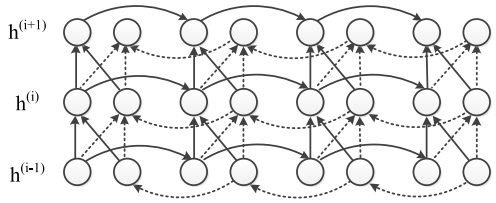

FIGURE 11. BiGRU structural model.

information $h_t^{(i-1)} = \left[\vec{h}_t^{(i-1)}; \overleftarrow{h}_t^{(i-1)}\right]$ passed from the upper hidden layer of the current moment. It includes information transmitted in both directions. The information propagated by the ith hidden layer to forward $\vec{h}_t^{(i)}$ and backward $\overleftarrow{h}_t^{(i)}$ is calculated as follows:

$$\vec{h}_t^{(i)} = f(\vec{W}^{(i)} h_t^{(i-1)} + \vec{V}^{(i)} \vec{h}_{t-1}^{(i)} + \vec{b}^{(i)}) \tag{14}$$

$$\overleftarrow{h}_t^{(i)} = f(\overleftarrow{W}^{(i)} h_t^{(i-1)} + \overleftarrow{V}^{(i)} \overleftarrow{h}_{t+1}^{(i)} + \overleftarrow{b}^{(i)}) \tag{15}$$

where f is the activation function, $\vec{W}^{(i)}$, $\vec{V}^{(i)}$ and $\vec{b}^{(i)}$ represent the two forward weights and biases of the ith layer respectively, $\overleftarrow{W}^{(i)}$, $\overleftarrow{V}^{(i)}$ and $\overleftarrow{b}^{(i)}$ represent the two backward weights and biases of the ith layer respectively.

ECG data is a typical time sequence that reflects the electrophysiological activity of the heart. The research on ECG mainly focused on the statistical characteristics of various waveforms, bands, and intervals of ECG in the past. This requires researchers to have certain professional medical knowledge. With the advancement of medical information, a large amount of ECG data has accumulated in the databases of hospitals and communities. How to extract potential effective features from massive data and classify test samples becomes a new topic. At present, there are a few studies [16], [44], [45] on the use of deep learning methods for the automatic extraction of ECG data [46], [47]. According to the characteristics of ECG time sequences, this paper proposes a new deep learning method, which can quickly and accurately determine whether MI and positioning according to ECG waveform. Detection and localization of MI is a sequence-to-sequence task. $X = [x_1, x_2, \cdots, x_m]$ represents a sequence of ECG signal after preprocessing and segmentation. It enters into the GRU deep learning network, then a label sequence $y = [y_1, y_2, \cdots, y_n]$ is exported. In the label sequence, y_i corresponds to one of the n types of MI, and only one of the n elements of the label sequence has a value of 1 and the rest are 0. In the training process, the parameters of the model are optimized by stochastic gradient descent (SGD). In order to improve the learning speed of the GRU network, the cross-entropy loss function is used to measure the closeness between the actual output and the expected output of the model. It is defined as:

$$C = -\frac{1}{n} \sum_x \left[y \ln \hat{y} + (1 - y) \ln \left(1 - \hat{y}\right) \right] \tag{16}$$

where y is the expected output, $\hat{y}$ is the actual output of the neuron, and n is the number of samples trained.

TABLE 4. Statistical table of diagnostic categories and number of subjects in PTB database.

Diagnostic class	Number of subjects
Myocardial infarction	148
Cardiomyopathy/Heart failure	18
Bundle branch block	15
Dysrhythmia	14
Myocardial hypertrophy	7
Valvular heart disease	6
Myocarditis	4
Miscellaneous	4
Healthy controls	52

Here, the SGD update process for parameters is mainly:

$$g_t = \nabla_{\theta_{t-1}} f(\theta_{t-1}) \tag{17}$$

$$\Delta\theta_t = -\eta g_t \tag{18}$$

where θ is the parameter to be optimized, η is the learning rate, and g_t is the gradient of SGD completely dependent on the current batch. The RELU activation function is used in the output layer of the model. The RELU uses a strong regularization method to train multi-layer deep neural networks, which makes the learning of the model robust, so there is no need to add any gradient cutting and regularization methods.

IV. EXPERIMENT & ANALYSIS

In order to verify the ML-BiGRU algorithm proposed in this paper, the experiment was completed according to the model architecture shown in Figure 9.

A. DATASET

The dataset used in this paper is the well-known PTB ECG diagnostic database, which is a digital ECG database provided by the National Metrology Institute of Germany. Its purpose is to research and teach algorithm standards. The data comes from the Department of Cardiology of University Clinic Benjamin Franklin in Berlin, Germany.

The PTB ECG diagnosis database includes 549 records of a total of 290 subjects with MI, cardiac hypertrophy, heart failure, bundle branch block, and healthy controls. The overall age ranges from 17 to 87, including 209 men (mean age 55.5), 81 women (mean age 61.6). One to five records is collected per subject. Each record is approximately 2 minutes and includes 15 simultaneously measured signals: traditional 12 leads together with 3 Frank lead ECG signals. The sampling frequency of the signal is 1000 Hz, the data storage format is Format16, and the resolution is 16 bits. The clinical summary is not available for 22 subjects, and the remaining 268 subjects had diagnostic conclusions. The diagnostic classes of the remaining 268 subjects are summarized in Table 4.

B. EXPERIMENTAL RESULT

1) EXPERIMENTAL PARAMETERS

First, the input ECG signal is denoised and preprocessed, then the R peak is located, and each ECG signal of about

TABLE 5. Parameter settings.

Parameter	Value
Samples_size	54753
Steps_num	1920
Batch_size	128
Hidden_num	64
Epochs_num	50
Dropout_rate	0.1
Classes_num	6

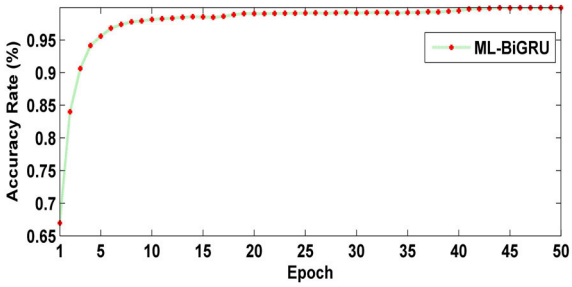

FIGURE 12. Experimental results with different epoch.

two minutes is segmented into a sequence of heartbeats. Each heartbeat takes 250ms and 400ms samples before and after R peak. The data constitutes a lead ECG vector. The 8 leads ECG signals are processed in the same manner to generate 8 ECG vectors. Each ECG vector is input into a BiGRU network for learning, and the results of 8 BiGRU network learning are input into a fully connected SoftMax layer to output classification results. The L2 regularization method is used to constrain the network parameters. The training process introduces the Dropout strategy to prevent over-fitting, and the batch SGD optimization method is used for model training. Hyper-parameters are one of the factors that affect the performance of the ML-BiGRU model system. The performance of the model will change with the value of hyper-parameters. The values of the hyper-parameters are shown in Table 5 and consist of samples_size, steps_num, batch_size, hidden_num, epochs_num, dropout_rate, classes_num. Before the start of the experiments, we analyze some sensitive parameters, and make a comparative experiment on the change of MI localization accuracy. The effect of the number of epoch and the batch size on accuracy is shown in Figure 12 and Figure 13 respectively. By training our model with the hyper-parameters listed in Table 5, we can obtain better localization results as mentioned in Section IV.C. The specific parameter settings are shown in Table 5.

2) PERFORMANCE METRICS

In order to evaluate the performance of the classification algorithm proposed in this paper, we used four statistical criteria: sensitivity (Sen), specificity (Spe), positive predictivity (Ppr) and accuracy (Acc). The classification accuracy evaluates the

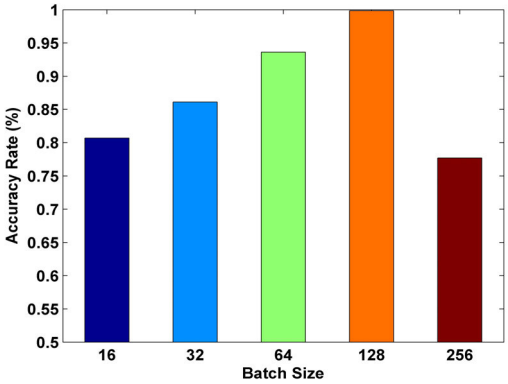

FIGURE 13. Experimental results with different batch size.

overall performance of the proposed method in all effective heartbeats. Sen, Spe, and Ppr have small deviations in evaluating classifier performance due to the different numbers of different types of heartbeats. The four statistical indicators can be calculated as follows:

$$Sen = \frac{TP}{TP + FN} \tag{19}$$

$$Spe = \frac{TN}{TN + FP} \tag{20}$$

$$Ppr = \frac{TP}{TP + FP} \tag{21}$$

$$Acc = \frac{TP + TN}{TP + FN + TN + FP} \tag{22}$$

where true positive (TP) is the number of heartbeats correctly detected as MI, true negative (TN) is the number of heartbeats correctly identified as HC, false negative (FN) is the number of heartbeats erroneously detected as HC, and false positive (FP) is the number of heartbeats erroneously diagnosed as MI.

C. DISCUSSIONS

During the training, the batch size is set to 128 and the number of training epochs is set to 50. All heartbeats are divided into 10 parts, 9 parts for training, and 1 part for testing. Division by category ensures that the distribution of classes in the subdataset is basically the same as that in the complete dataset, so as to avoid the situation that some classes are not adequately trained because of the lack of samples. The confusion matrix and classification performance results are summarized in Table 6. The overall accuracy of the algorithm in MI classification is 99.84%, and the accuracy in the ASMI and ILMI categories is 99.98%. In addition, the accuracy of the IMI and ALMI categories is slightly lower than in other categories. This is because there is a small number of IMI and HC and ILMI samples with a high degree of similarity in waveform morphology, which is difficult to distinguish. Because the ALMI class has fewer heartbeat samples, deep learning models usually requires more data to get better results. However, the average accuracy of IMI and ALMI is still as high as 99.89%, which is acceptable, so there is no other complicated data processing work to further improve performance. Also,

TABLE 6. Confusion matrix and classification performance of ML-BiGRU.

True Class	Predicted Class						Classification Performance			
	AMI	ALMI	ASMI	IMI	ILMI	HC	Sen	Spe	Ppr	Acc
AMI	621	1	0	0	0	0	0.9984	0.9998	0.9984	0.9996
ALMI	1	634	1	2	0	0	0.9937	0.9996	0.9969	0.9989
ASMI	0	0	1168	0	0	0	1.0000	0.9998	0.9991	0.9998
IMI	0	1	0	1245	0	1	0.9984	0.9991	0.9968	0.9989
ILMI	0	0	0	1	729	0	0.9986	1.0000	1.0000	0.9998
HC	0	0	0	1	0	1069	0.9991	0.9998	0.9991	0.9996

TABLE 7. Confusion matrix and classification performance of literature 33.

True Class	Predicted Class						Classification Performance			
	AMI	ALMI	ASMI	IMI	ILMI	HC	Sen	Spe	Ppr	Acc
AMI	7316	4	6	7	2	1	0.9973	0.9996	0.9973	0.9993
ALMI	9	6843	12	5	8	0	0.9951	0.9998	0.9982	0.9992
ASMI	5	2	11956	4	1	3	0.9987	0.9995	0.9979	0.9993
IMI	5	3	1	13512	10	0	0.9986	0.9994	0.9981	0.9992
ILMI	0	1	3	8	8962	1	0.9986	0.9995	0.9974	0.9994
HC	1	2	3	2	2	10636	0.9991	0.9999	0.9995	0.9997

TABLE 8. Confusion matrix and classification performance of literature 30.

True Class	Predicted Class						Classification Performance			
	AMI	ALMI	ASMI	IMI	ILMI	HC	Sen	Spe	Ppr	Acc
AMI	489	1	8	0	0	2	0.9780	0.9942	0.9722	0.9914
ALMI	2	438	2	0	0	0	0.9910	0.9976	0.9865	0.9966
ASMI	9	2	488	0	0	1	0.9760	0.9942	0.9721	0.9911
IMI	1	0	2	487	9	1	0.9740	0.9971	0.9858	0.9932
ILMI	1	2	0	7	490	0	0.9800	0.9963	0.9820	0.9935
HC	1	1	2	0	0	476	0.9917	0.9984	0.9917	0.9973

the algorithm achieves more than 99% sensitivity, specificity, and accuracy in all categories. The confusion matrices and classification performance of literature 30 and 33 are shown in Table 7 and 8 respectively. According to the Table 6, 7, and 8, we can see that the performance of this paper and literature 33 are obviously higher than that of literature 30. The reason is that both this paper and literature 33 adopt the method of deep learning to extract features automatically, and the effectiveness of features is better than that of hand-crafted features used in literature 30. T-test results of two independent samples shows that ML-BiGRU achieved better performance than the method in [33] on Sen, Spe, Ppr, Acc. But there is no significant performance difference (P value > 0.05). However, the accuracy of ML-BiGRU is higher than that of the method in [30], and there is a very significant performance difference between them (P value < 0.01). By observing the waveforms of the six types of heartbeat in Figure 8, we can see that the amplitudes of QRS complex waveforms of ALMI, IMI and HC change rapidly and the waveforms are steep. CNN classification method is more suitable for this situation. The QRS complex waves of AMI, ASMI, and ILMI are relatively flat. ML-BiGRU is more suitable.

Next, compare some performance of the methods proposed in this paper with other literature, are shown in Table 9. The following are listed in the table: the number of MIs that can be identified, the method of feature extraction, and the methods used, the classifier used and the average performance. The methods listed in Table 9 all use the same ECG database PTB as the experimental dataset. The accuracy of the proposed method in this paper is significantly higher than that of other literature in Table 9. Padhy and Dandapat [30] propose a tensor-based classification method for MI. First, denoise preprocessing is performed on the ECG signal; the heartbeat segmentation is implemented; the correlation between the continuous heartbeats and multi-lead is utilized; the high-order singular value decomposition (HOSVD) method is used

TABLE 9. ML-BiGRU performance comparison with other literature.

Author(Year)	# of classes	Feature Set	Classifier	MI localization
Tahsin Reasat et al.(2017) [26]	2	End-to-end	CNN	Acc=84.54% Sen=85.33% Spe=84.09%
Hin Wai LUI et al. (2018) [20]	4	End-to-end	CNN-LSTM	Sen=92.4% Spe=97.7% Ppr=97.2%
Nils Strodthoff et al.(2018) [32]	2	End-to-end	CNN	Sen=93.3% Spe=89.7% Ppr=93.6%
U. Rajendra Acharya et al.(2017) [21]	2	End-to-end	CNN	Acc=95.22% Sen=95.49% Spe=94.19%
Sibasankar et al.(2017) [30]	6	DWT	SVM	Acc=98.15%
U. Rajendra et al.(2016) [29]	11	DWT	KNN	Acc=98.74% Sen=99.55% Spe=99.16%
Arif M et al.(2012) [36]	11	DWT	KNN	Acc=98.8%
L. N. Sharma et al.(2015) [31]	7	DWT	SVM	Acc=99.58%
Wenhan Liu et al.(2018) [33]	6	End-to-end	CNN	Acc=99.81%
ML-BiGRU	**6**	**End-to-end**	**BiGRU**	**Acc=99.84%**

to extract features from the multi-lead ECG third-order tensor, and finally, a multi-class SVM classifier is used. The classification accuracy of MI reaches 98.15%.

Rajendra *et al.* [29] first denoise the ECG signal; realize the heartbeat segmentation; perform the discrete wavelet transform to obtain the transform coefficients; manually extract the nonlinear features and finally use the KNN classifier. 10 categories MI and normal heartbeats are classified. Although this method only uses the data of the V3 lead, the ECG signal can be better characterized than the linear feature, because this method transforms the ECG signal from the time domain to the frequency domain and extracts nonlinear feature manually from the ECG signal. The average accuracy reaches 98.74%.

Arif *et al.* [36] first detect the QRS complex using discrete wavelet transform and extract several time domain features from the 12-lead ECG signals, such as Q-wave amplitude, T-wave amplitude, and ST-segment level offset. Then MI is classified by the KNN method and finally, the performance of the algorithm is verified on the PTB database. Although only a few hand-crafted features are extracted in the time domain, this method uses the 12-lead ECG signals, so the acquired features are more comprehensive and effective. According to the confusion matrix, the accuracy of MI localization reaches 98.8%.

Sharma *et al.* [31] propose a multi-scale energy and feature space method to detect and locate MI from multi-lead ECG signals. For the multi-lead ECG data, the preprocessing is firstly performed, and the discrete wavelet transform is used to extract the multi-scale wavelet energy and the multi-scale covariance matrix eigenvalues as features. Finally, the SVM classifier is used to detect and locate the MI. The accuracy of the algorithm in MI localization reaches 99.58%.

Liu *et al.* [33] propose a new method of multi-feature branch CNN in 2018 to detect and locate MI. Each feature branch corresponds to a lead of the ECG; learns the difference between the 12 leads; summarizes the learning results of all the feature branches, and obtains the classification result by using the fully connected Softmax classifier. Using the PTB ECG database, after preprocessing and automatically extracting features by combining 12-lead ECG data, and the average accuracy of MI localization is 99.81%.

The proposed algorithm in this paper denoises the original ECG signal and analyzes the comprehensive multi-lead data. The BiGRU deep learning method is adopted, which is not limited to the manual features designed by medical experts. With useful information hidden behind big data, the machine automatically extracts features and achieves excellent results in MI localization. This paper classifies the PTB ECG signal on the TensorFlow platform. The platform integrates deep learning models such as CNN, RNN, LSTM, and GRU. The CPU is Intel Core i7-7700, the memory is 32GB, and the GPU is NVIDIA GeForce GTX 1080. The memory of GPU is 8GB. The operating system is 64-bit Windows 10.

V. CONCLUSION

In this paper, a BiGRU-based multi-lead MI detection and classification algorithm is proposed. Firstly, the ECG signal is preprocessed by the filter bank; the Pan-Tompkins algorithm is used to locate the R wave and then each ECG signal is

segmented into independent heartbeats; finally, the BiGRU deep learning method is used to extract features automatically and implement the localization of MI. The algorithm is validated on the public PTB ECG database, and the experimental results are compared with other algorithms. The results show that the proposed algorithm has higher sensitivity, positive predictivity, accuracy, and universality. The potentially useful features can be extracted from the multi-lead ECG signals using the deep learning framework proposed herein. The method proposed in this paper can be further extended to achieve multi-class classification tasks similar to this one. Further work can be explored to train the classifier on other ECG datasets to detect a variety of other heart diseases. Considering its excellent performance, the BiGRU-based multi-lead MI detection and localization algorithm can be applied to computer-aided diagnosis platform. Compared with traditional methods, the disadvantage of this algorithm is the long training time. How to improve the training speed on the premise of ensuring the accuracy is the future research topic.

REFERENCES

[1] K. Thygesen, J. S. Alpert, A. S. Jaffe, M. L. Simoons, B. R. Chaitman, and H. D. White, "Third universal definition of myocardial infarction," *Circulation*, vol. 126, no. 16, pp. 2020–2035, 2012.

[2] E. Boersma, A. C. P. Maas, J. W. Deckers, and M. L. Simoons, "Early thrombolytic treatment in acute myocardial infarction: Reappraisal of the golden hour," *Lancet*, vol. 348, no. 9030, pp. 771–775, 1996.

[3] P. Valensi, L. Lorgis, and Y. Cottin, "Prevalence, incidence, predictive factors and prognosis of silent myocardial infarction: A review of the literature," *Arch. Cardiovascular Diseases*, vol. 104, no. 3, pp. 178–188, 2011.

[4] Y. LeCun, Y. Bengio, and G. Hinton, "Deep learning," *Nature*, vol. 521, pp. 436–444, May 2015.

[5] A. Krizhevsky, I. Sutskever, and G. E. Hinton, "ImageNet classification with deep convolutional neural networks," in *Proc. Adv. Neural Inf. Process. Syst. (NIPS)*, 2012, pp. 1097–1105.

[6] K. Simonyan and A. Zisserman, "Very deep convolutional networks for large-scale image recognition," 2015, *arXiv:1409.1556*. [Online]. Available: https://arxiv.org/abs/1409.1556

[7] J. Donahue, L. A. Hendricks, M. Rohrbach, S. Venugopalan, S. Guadarrama, K. Saenko, and T. Darrell, "Long-term recurrent convolutional networks for visual recognition and description," *IEEE Trans. Pattern Anal. Mach. Intell.*, vol. 39, no. 4, pp. 677–691, Apr. 2017.

[8] A. Ullah, J. Ahmad, K. Muhammad, M. Sajjad, and S. W. Baik, "Action recognition in video sequences using deep bi-directional LSTM with CNN features," *IEEE Access*, vol. 6, pp. 1155–1166, Nov. 2017.

[9] G. Zhu, L. Zhang, P. Shen, and J. Song, "Multimodal gesture recognition using 3-D convolution and convolutional LSTM," *IEEE Access*, vol. 5, pp. 4517–4524, Mar. 2017.

[10] D. Amodei *et al.*, "Deep speech 2: End-to-end speech recognition in english and mandarin," 2015, *arXiv:1512.02595*. [Online]. Available: https://arxiv.org/abs/1512.02595

[11] R. Zazo, P. S. Nidadavolu, N. Chen, J. Gonzalez-Rodriguez, and N. Dehak, "Age estimation in short speech utterances based on LSTM recurrent neural networks," *IEEE Access*, vol. 6, pp. 22524–22530, Mar. 2018.

[12] Y. Yuan, C. Tian, and X. Lu, "Auxiliary loss multimodal GRU model in audio-visual speech recognition," *IEEE Access*, vol. 6, pp. 5573–5583, Feb. 2018.

[13] G. Litjens, T. Kooi, B. E. Bejnordi, A. A. A. Setio, F. Ciompi, M. Ghafoorian, J. A. van der Laak, B. van Ginneken, and C. I. Sánchez, "A survey on deep learning in medical image analysis," *Med. Image Anal.*, vol. 42, pp. 60–88, Dec. 2017.

[14] A. Esteva, B. Kuprel, R. A. Novoa, J. Ko, S. M. Swetter, H. M. Blau, and S. Thrun, "Dermatologist-level classification of skin cancer with deep neural networks," *Nature*, vol. 542, pp. 115–118, Feb. 2017.

[15] P. Rajpurkar, A. Y. Hannun, M. Haghpanahi, C. Bourn, and Y. A. Ng, "Cardiologist-level arrhythmia detection with convolutional neural networks," 2017, *arXiv:1707.01836*. [Online]. Available: https://arxiv.org/abs/1707.01836

[16] X. Zhai and C. Tin, "Automated ECG classification using dual heartbeat coupling based on convolutional neural network," *IEEE Access*, vol. 6, pp. 27465–27472, 2018.

[17] D. Sopic, A. Aminifar, A. Aminifar, and D. Atienza, "Real-time event-driven classification technique for early detection and prevention of myocardial infarction on wearable systems," *IEEE Trans. Biomed. Circuits Syst.*, vol. 12, no. 5, pp. 982–992, Jul. 2018.

[18] M. Sharma, R. S. Tan, and U. R. Acharya, "A novel automated diagnostic system for classification of myocardial infarction ECG signals using an optimal biorthogonal filter bank," *Comput. Biol. Med.*, vol. 102, pp. 341–356, Nov. 2018.

[19] A. Dĺker, Z. Cömert, and E. Avci, "A diagnostic model for identification of myocardial infarction from electrocardiography signals," *J. Sci. Technol.*, vol. 7, no. 2, pp. 132–139, 2017.

[20] H. W. Lui and K. L. Chow, "Multiclass classification of myocardial infarction with convolutional and recurrent neural networks for portable ECG devices," *Inform. Med. Unlocked*, vol. 13, pp. 26–33, Jan. 2018.

[21] U. R. Acharya, H. Fujita, S. Oh, Y. Hagiwara, J. H. Tan, and M. Adam, "Application of deep convolutional neural network for automated detection of myocardial infarction using ECG signals," *Inf. Sci.*, vol. 415, pp. 190–198, Nov. 2017.

[22] S. Banerjee and M. Mitral, "ECG feature extraction and classification of anteroseptal myocardial infarction and normal subjects using discrete wavelet transform," in *Proc. Int. Conf. Syst. Med. Biol.*, Dec. 2010, pp. 55–60.

[23] A. K. Dohare, V. Kumar, and R. Kumar, "Detection of myocardial infarction in 12 lead ECG using support vector machine," *Appl. Soft Comput.*, vol. 64, pp. 138–147, Mar. 2018.

[24] P.-C. Chang, J.-J. Lin, J.-C. Hsieh, and J. Weng, "Myocardial infarction classification with multi-lead ECG using hidden Markov models and Gaussian mixture models," *Appl. Soft Comput.*, vol. 12, no. 10, pp. 3165–3175, 2012.

[25] N. A. Bhaskar, "Performance analysis of support vector machine and neural networks in detection of myocardial infarction," *Procedia Comput. Sci.*, vol. 46, pp. 20–30, Jan. 2015.

[26] T. Reasat and C. Shahnaz, "Detection of inferior myocardial infarction using shallow convolutional neural networks," in *Proc. IEEE Region 10 Humanitarian Technol. Conf.*, Dec. 2017, pp. 718–721.

[27] S. Khatun and B. I. Morshed, "Detection of myocardial infarction and arrhythmia from single-lead ECG data using bagging trees classifier," in *Proc. IEEE Int. Conf. Electro Inf. Technol. (EIT)*, May 2017, pp. 520–524.

[28] H. Yang, S. T. S. Bukkapatnam, T. Le, and R. Komanduri, "Identification of myocardial infarction (MI) using spatio-temporal heart dynamics," *Med. Eng. Phys.*, vol. 34, no. 4, pp. 485–497, 2012.

[29] U. R. Acharya, H. Fujita, V. K. Sudarshan, S. L. Oh, M. Adam, J. E. Koh, J. H. Tan, D. N. Ghista, R. J. Martis, C. K. Chua, C. K. Poo, and R. S. Tan, "Automated detection and localization of myocardial infarction using electrocardiogram: A comparative study of different leads," *Knowl.-Based Syst.*, vol. 99, pp. 146–156, May 2016.

[30] S. Padhy and S. Dandapat, "Third-order tensor based analysis of multilead ECG for classification of myocardial infarction," *Biomed. Signal Process. Control*, vol. 31, pp. 71–78, Jan. 2017.

[31] L. N. Sharma, R. K. Tripathy, and S. Dandapat, "Multiscale energy and eigenspace approach to detection and localization of myocardial infarction," *IEEE Trans. Biomed. Eng.*, vol. 67, no. 7, pp. 1827–1837, Feb. 2015.

[32] N. Strodthoff and C. Strodthoff, "Detecting and interpreting myocardial infarction using fully convolutional neural networks," 2018, *arXiv:1806.07385*. [Online]. Available: https://arxiv.org/abs/1806.07385

[33] W. Liu, Q. Huang, S. Chang, H. Wang, and J. He, "Multiple-feature-branch convolutional neural network for myocardial infarction diagnosis using electrocardiogram," *Biomed. Signal Process. Control*, vol. 45, pp. 22–32, Aug. 2018.

[34] J. F. Wu, Y. L. Bao, S. C. Chan, H. C. Wu, L. Zhang, and X. G. Wei, "Myocardial infarction detection and classification—A new multi-scale deep feature learning approach," in *Proc. IEEE Int. Conf. Digit. Signal Process. (DSP)*, Oct. 2016, pp. 309–313.

[35] L. Sun, Y. Lu, K. Yang, and S. Li, "ECG analysis using multiple instance learning for myocardial infarction detection," *IEEE Trans. Biomed. Eng.*, vol. 59, no. 12, pp. 3348–3356, Aug. 2012.

[36] M. Arif, I. A. Malagore, and F. A. Afsar, "Detection and localization of myocardial infarction using k-nearest neighbor classifier," *J. Med. Syst.*, vol. 36, no. 1, pp. 279–289, 2012.
[37] J. Pan and W. J. Tompkins, "A real-time QRS detection algorithm," *IEEE Trans. Biomed. Eng.*, vol. BME-32, no. 3, pp. 230–236, Mar. 1985.
[38] M. Hammad, A. Maher, K. Wang, F. Jiang, and M. Amrani, "Detection of abnormal heart conditions based on characteristics of ECG signals," *Measurement*, vol. 125, pp. 634–644, Sep. 2018.
[39] A. Bharadwaj and U. Kamath, "Techniques for accurate ECG signal processing," *EE Times*, vol. 14, pp. 1–7, Feb. 2011.
[40] W. Einthoven, G. Fahr, and A. De Waart, "On the direction and manifest size of the variations of potential in the human heart and on the influence of the position of the heart on the form of the electrocardiogram," *Amer. Heart J.*, vol. 40, no. 2, p. 163, 1950.
[41] M. Oehler, M. Schilling, and H. D. Esperer, "Novel multichannel capacitive ECG-System for cardiac diagnostics beyond the standard-lead system," in *Proc. 4th Eur. Conf. Int. Fed. Med. Biol. Eng.* Berlin, Germany: Springer, 2009, pp. 30–33.
[42] S. Hochreiter and J. Schmidhuber, "Long short-term memory," *Neural Comput.*, vol. 9, no. 8, pp. 1735–1780, 1997.
[43] J. Chung, C. Gulcehre, K. Cho, and Y. Bengio, "Empirical evaluation of gated recurrent neural networks on sequence modeling," 2014, *arXiv:1412.3555*. [Online]. Available: https://arxiv.org/abs/1412.3555
[44] M. Hammad, Y. Liu, and K. Wang, "Multimodal biometric authentication systems using convolution neural network based on different level fusion of ECG and fingerprint," *IEEE Access*, vol. 7, pp. 26527–26542, 2019.
[45] M. Amrani, M. Hammad, F. Jiang, K. Wang, and A. Amrani, "Very deep feature extraction and fusion for arrhythmias detection," *Neural Comput. Appl.*, vol. 30, no. 7, pp. 2047–2057, Oct. 2018.
[46] Q. Zhang, D. Zhou, and X. Zeng, "HeartID: A multiresolution convolutional neural network for ECG-based biometric human identification in smart health applications," *IEEE Access*, vol. 5, pp. 11805–11816, 2017.
[47] M. Hammad, "A novel deep transfer learning method for detection of myocardial infarction," 2019, *arXiv:1906.09358*. [Online]. Available: https://arxiv.org/abs/1906.09358

XINGJIN ZHANG received the B.E. and M.E. degrees in computer science from the School of Information Engineering, Zhengzhou University, China, in 1997 and 2005, respectively. He is currently pursuing the Ph.D. degree with the State Key Laboratory of Mathematical Engineering and Advanced Computing, Zhengzhou, China. Since 1997, he has been with the Faculty of the School of Information Engineering, Zhengzhou University, where he is also a Lecturer in computer science. He is also a Researcher with the Cooperative Innovation Center of Internet Healthcare, Zhengzhou University. His research interests include machine learning and healthcare big data.

RUNCHUAN LI received the B.S. degree in computer science from Zhengzhou University, China, in 2015. He is currently pursuing the Ph.D. degree with Zhengzhou University, where he is also a Researcher with the Cooperative Innovation Center of Internet Healthcare. His research interests include machine learning, data mining, and artificial intelligence.

HONGHUA DAI received the M.Sc. degree from the Graduate School, Chinese Academy of Sciences, in 1986, and the Ph.D. degree from the Department of Computer Science, RMIT University, in 1994. He was a Research Fellow with the Department of Computer Science, Monash University, from 1994 to 1997. He joint Deakin University, in 1999. He is currently a specially-appointed Professor with the Cooperative Innovation Center of Internet Healthcare, Zhengzhou University. His recent research interests include minimum message length principle-based causal discovery, inexact field learning approach, reliable knowledge discovery, big data intelligence, machine learning for weather forecasting, data mining, and artificial intelligence and intelligence healthcare. He is a member of ACM and the IEEE computer society.

YONGPENG LIU received the B.S. and M.S. degrees in computer science from the Information Engineering School, Zhengzhou University, China, in 2010 and 2013, respectively. He is currently pursuing the Ph.D. degree with Zhengzhou University, where he is also a Researcher with the Cooperative Innovation Center of Internet Healthcare. His research interests include wise medicine, machine learning, and data mining.

BING ZHOU was born in Shangqiu, Henan. He received the master's degree in computer science from Xi'an Jiaotong University, in June 1989, and the Ph.D. degree in computer science from the Beijing University of Aeronautics and Astronautics, in March 2003. From November 2006 to November 2007, he was a Visiting Scholar with the University of Washington. Since 2003, he has been a Professor and a Doctoral Tutor with Zhengzhou University. His main research interests include intelligent diagnosis of ECG, computer vision, the Internet medical, and computer networks.

ZONGMIN WANG was born in Zhengzhou, Henan. He received the Ph.D. degree in engineering from Tsinghua University, in March 1996. From 1996 to 1997, he went to the University of Hong Kong for collaborative scientific research. From 1997 to 2017, he served as a Professor and a Doctoral Tutor with Zhengzhou University, where he also served as the Vice President, from August 2008 to August 2017. From January 2010 to July 2010, he served as a Senior Research Scholar with the University of Memphis. Since September 2017, he has been the President of the Zhongyuan University of Technology. He is currently the Director of the Cooperative Innovation Center of Internet Healthcare, Zhengzhou University. His main research interests include intelligent diagnosis of ECG, the Internet medical, and computer networks.